

# First-principles study on the negative- $U$ behavior of $K$ centers in amorphous $\text{Si}_3\text{N}_{4-x}$

Gijae Kang,<sup>1</sup> Dongheon Lee,<sup>1</sup> Kyeongpung Lee,<sup>1</sup> Jeenu Kim,<sup>2</sup> and Seungwu Han<sup>1,\*</sup>

<sup>1</sup>*Department of Materials Science and Engineering and Research Institute of Advanced Materials, Seoul National University, Seoul 08826, South Korea*

<sup>2</sup>*R&D Division, SK Hynix Inc., Icheon-si, Gyeonggi-do 17336, South Korea*

(Received 1 August 2018; revised manuscript received 18 October 2018; published 20 December 2018)

We investigate the charge-trapping behavior in nitrogen-deficient amorphous silicon nitride ( $a\text{-Si}_3\text{N}_{4-x}$ ) using first-principles calculations. The amorphous ensembles with one nitrogen atom missing are generated through melt-quench procedures. The nitrogen deficiency mainly produces one Si—Si bond and one  $K$  center (Si dangling bond). The energy level of defect states indicates that the  $K$  centers act as possible trap sites. The transition levels of  $K$  centers are estimated, and it is found that the Hubbard  $U$  energy ranges from  $-1.14$  to  $1.11$  eV. Even though most  $K$  centers show positive  $U$ , the charge states of most centers in the ensemble are either positive or negative under the charge-neutrality condition, resulting in “seemingly negative- $U$ ” behavior. This is consistent with the diamagnetic signal in experiments. The charge-injection energy of  $K$  centers is evaluated on the basis of the Franck-Condon approximation, and the average trap depths for electrons (1.33 eV below the conduction edge) and holes (1.54 eV above the valence edge) are in good agreement with experimental data.

DOI: [10.1103/PhysRevApplied.10.064052](https://doi.org/10.1103/PhysRevApplied.10.064052)

## I. INTRODUCTION

As society shifts toward data-intensive electronic lifestyles, the consumer market for nonvolatile memory has grown steeply over the last decade, which also increased the need to address technical challenges such as scaling limitation and reliability of the nonvolatile memory [1–5]. In the traditional floating-gate memory, to prevent charge losses that degrade the data retention, the thickness of tunneling oxides should be at least 8 nm, otherwise even a single trap in the oxide could result in complete loss of charges [1]. This requirement for the minimum oxide thickness is critically limiting the downscaling of flash-memory devices.

One solution to the charge-loss problem is to store the charges at spatially localized sites in a charge-trap layer rather than over the whole gate volume. Such a device structure is called “charge-trap flash (CTF) memory.” The trapped charges are immobile and spatially well separated from defects in the gate or tunneling oxides, thereby suppressing the trap-assisted tunneling. With the superior retention property, CTF memory is rapidly replacing the conventional floating-gate memory in high-density solid-state drives [5,6].

In CTF memory, N-deficient, nonstoichiometric amorphous silicon nitrides ( $a\text{-Si}_3\text{N}_{4-x}$ ) are used as the

material for the charge-trap layer. The nonstoichiometry of  $a\text{-Si}_3\text{N}_{4-x}$  creates many localized defect levels inside a wide band gap of 4.6 eV. The localized nature of midgap states in  $a\text{-Si}_3\text{N}_{4-x}$  immobilizes electrons in the charge-trap layer, which reduces the leakage current and hence improves the retention property. The invention of CTF memory dates back to the 1960s when the metal-nitride-oxide-silicon structure using  $a\text{-Si}_3\text{N}_{4-x}$  was studied. Soon after the carrier trapping under an electric bias and temperature stress was first observed, the memory behavior of the metal-nitride-oxide-silicon device was demonstrated [7–10].

In spite of the long history and wide use in commercial devices, the atomistic origin of the trap states in  $a\text{-Si}_3\text{N}_{4-x}$  is still elusive, which could be a hurdle preventing further engineering of the material property and improving device performances. In the stoichiometric crystalline structure of  $\beta\text{-Si}_3\text{N}_4$  (crystalline  $\text{Si}_3\text{N}_4$ ,  $c\text{-Si}_3\text{N}_4$ ), Si and N atoms are coordinated by four and three counterions, respectively, and such local structures are well preserved in the amorphous phases [11]. Therefore, the dangling bond of Si atoms, called the “ $K$  center,” would be the major defect in N-deficient samples, and many studies assumed  $K$  centers as the primary trap sites in  $a\text{-Si}_3\text{N}_{4-x}$  [12–14].

As is well established in Si and  $a\text{-Si}$  [15–17], the dangling bond of Si is a paramagnetic center in its neutral state due to the unpaired electron, which can be detected by electron-spin-resonance (ESR) measurement. However,

\*hansw@snu.ac.kr

only weak ESR signals were observed for  $a\text{-Si}_3\text{N}_{4-x}$  [18,19], which is at variance with the  $K$  center as the major trap site. One way to explain the absence of an ESR signal is to assume a negative Hubbard repulsion energy of the  $K$  center, or so-called negative  $U$ , which charges  $K$  centers through a spontaneous reaction of  $K^0 + K^0 \rightarrow K^+ + K^-$ . At thermal equilibrium, the dangling bonds are either doubly occupied ( $K^-$ ) or empty ( $K^+$ ) such that they do not produce any ESR signal because of the diamagnetic nature. Several studies combining ESR and UV illumination supported the negative- $U$  model of trap centers in  $a\text{-Si}_3\text{N}_{4-x}$ ; while UV illumination generated neutral  $K^0$  centers detectable by ESR measurement, they were metastable in the ambient condition and transformed into diamagnetic  $K^+$  and  $K^-$  centers after short annealing, supporting the negative- $U$  character of the trap [18–24].

The negative- $U$  property of  $K$  centers can be directly investigated by density-functional-theory (DFT) calculations. Since modeling on the amorphous structure is costly, many studies investigated alternatively the N vacancy in  $c\text{-Si}_3\text{N}_4$  [2,25–32]. In  $c\text{-Si}_3\text{N}_4$ , removal of one N atom results in three Si dangling bonds, and the structural relaxation makes two of them form a weak Si—Si bond, leaving one  $K$  center [26,29–31]. The localized states associated with this  $K$  center were identified within the band gap [12,25,29,31]. The computed transition level displayed negative- $U$  behavior ( $U \sim -0.1$  eV) as  $K^0$  is always less stable than  $K^+$  or  $K^-$  over the entire range of the Fermi level. In some studies, the weak Si—Si bond, which is formed by the local relaxation of two Si dangling bonds (the bond length is reduced from 3.05 to 2.64 Å), was suggested as a possible trap site [26,29,30,33].

In the present study, we pay attention to the possibility that the local environment around the  $K$  center in  $a\text{-Si}_3\text{N}_{4-x}$  can be different from that in  $c\text{-Si}_3\text{N}_4$ . The small magnitude of  $U$  of 0.1 eV suggests that the polarity of  $U$  could be reversed in  $a\text{-Si}_3\text{N}_{4-x}$ . Furthermore, the Si—Si bond length of 2.64 Å around the  $K$  center in  $c\text{-Si}_3\text{N}_4$  is much longer than that in crystalline Si (2.35 Å), which is a consequence of the defect embedded in the crystalline matrix. In the amorphous phase, such a constraint is relieved, and a different defect level can result. The foregoing discussion concludes that the atomistic model of the trap site in  $a\text{-Si}_3\text{N}_{4-x}$  that is consistent with findings from EPR experiments is not confirmed yet. In particular, the proposed negative- $U$  behavior of the  $K$  center is still questionable. There are a multitude of classical and DFT simulations on stoichiometric  $a\text{-Si}_3\text{N}_4$  and nonstoichiometric  $a\text{-Si}_3\text{N}_{4-x}$  [34–41], but detailed analysis of the charge-trapping behavior of the defect states in amorphous structures is missing.

In this work, we perform DFT calculations on stoichiometric  $a\text{-Si}_3\text{N}_4$  and N-deficient  $a\text{-Si}_3\text{N}_{4-x}$ . Ensembles of amorphous structures are generated by DFT molecular-dynamics (MD) simulations, and the atomic configurations

and electronic properties of trap states in  $a\text{-Si}_3\text{N}_{4-x}$  are analyzed. In most of  $a\text{-Si}_3\text{N}_{4-x}$ , the nitrogen deficiency results in a  $K$  center and a Si—Si bond. By calculating the formation energies of neutral and charged  $K$  centers, we find that the  $K$  center in amorphous structures has  $U$  ranging over positive as well as negative values, which is due to the fluctuation in the local environment of the  $K$  centers. In the ensemble of  $K$  centers, the Fermi level is determined from the charge-neutrality condition, and it is found that most  $K$  centers are charged positively or negatively, yielding a seemingly negative- $U$  behavior. Finally, the charge-trap levels for electrons and holes are calculated on the basis of the Franck-Condon approximation, and they are in good agreement with experimental data.

## II. COMPUTATIONAL METHODS

### A. Computational setup

We perform first-principles calculations using the Vienna Ab initio Simulation Package. [42–44] The generalized-gradient approximation with the Perdew-Burke-Ernzerhof (PBE) functional is used for the exchange-correlation energy of electrons [45]. During the melt-quench MD simulations to generate amorphous structures, we use a soft pseudopotential for N atoms, which reduces the energy cutoff for the plane-wave basis to 250 eV. Only the  $\Gamma$  point is selected for the  $\mathbf{k}$ -point sampling during MD simulations, and the time step is set to 2 fs. At the end of the melt-quench process, the lattice vectors and atomic positions are relaxed with use of the standard pseudopotential with an energy cutoff of 500 eV until the atomic forces and stress tensors are reduced to within 0.02 eV/Å and 2 kbar, respectively. The total energy and the electronic structure are calculated with an energy cutoff of 500 eV and  $\mathbf{k}$  points sampled on the  $3 \times 3 \times 3$  grid. The spin-polarized calculation is performed when one N atom is removed because of the local spin moment at the dangling bond. When an accurate description of the band gap is necessary, we perform additional atomic relaxations with the HSE06 hybrid functional [46]. In this case, only the  $\Gamma$  point is sampled for the Brillouin-zone integration to reduce the computational cost.

### B. Modeling amorphous structures

We obtain amorphous structures of  $a\text{-Si}_3\text{N}_4$  through the conventional melt-quench process [47]. The initial atomic positions are generated by randomly distributing atoms. The stoichiometric  $a\text{-Si}_3\text{N}_4$  supercells consist of 48 Si atoms and 64 N atoms while the supercell for N-deficient  $a\text{-Si}_3\text{N}_{4-x}$  includes 48 Si atoms and 63 N atoms ( $x = 0.0625$ ). In many theoretical studies, the stoichiometric amorphous structure was obtained through the melt-quench process and defects were generated by removal of atoms from the stoichiometric model. We think that such a

postremoval scheme is at variance with the nature of amorphous structures that the atomic sites are ill-defined. Therefore, we include the nitrogen vacancy from the beginning of the melt-quench process.

In choosing the mass density, we note that various studies reported sample densities of 2.4–3.2 g/cm<sup>3</sup> [11,48–51]. (The corresponding value for *c*-Si<sub>3</sub>N<sub>4</sub> is 3.18 g/cm<sup>3</sup>.) The large variation in the amorphous density stems from the wide range of nitrogen deficiency; in Ref. [39], it was found that the average volume per atom linearly depends on the nitrogen concentration. We are simulating a structure close to the nominal stoichiometry (Si:N ratio of 3:4), and the density for this composition is estimated to be 3.14 g/cm<sup>3</sup> according to the linear relation. In addition, DFT energies of *a*-Si<sub>3</sub>N<sub>4</sub> with different densities were studied in Ref. [52], and the lowest energy was obtained with 3.10 g/cm<sup>3</sup>. Therefore, we use 3.10 g/cm<sup>3</sup> for the initial density in the simulation.

Each structure is premelted at 5000 K for 5 ps to erase the initial information of the random positions. The liquid is then equilibrated at 3000 K for 10 ps, and quenched to 2000 K with a cooling rate of 33 K/ps. When the temperature is lower than 2000 K, the atoms vibrate only locally around the equilibrium point due to the strong Si—N bond, which means that further quenching is not necessary. Finally, the structure undergoes atomic relaxation, including optimization of lattice vectors (i.e., both the cell shape and the cell volume are fully relaxed). The average density of the final structures is 3.10 ± 0.037 g/cm<sup>3</sup>, almost identical to the starting value and within the experimental data (see above). Care should be taken during the quenching simulation since N<sub>2</sub> molecules are easily formed when the quenching speed is too fast. Because of the strong N—N bonding, the N<sub>2</sub> molecules do not break for the rest of the simulation. With a quenching rate of 33 K/ps, only two of 40 samples contain N—N bonding, while faster quenching yields more N—N bonding (up to 63% of samples contain N<sub>2</sub> molecules if a quenching rate of 540 K/ps is used).

### C. Defect formation energy

We consider a charge state (*q*) of −1, 0, +1 for the *K* center and calculate the formation energy of charged defects (*E*<sub>f</sub><sup>q</sup>) as follows:

$$E_f^q = E^q - E^0 + q(E_V + E_F) + E_{\text{corr}} + \mu_N, \quad (1)$$

where *E*<sup>q</sup> and *E*<sup>0</sup> are the total energies of the nonstoichiometric cell with charge *q* and the perfect cell with zero charge, respectively, *E*<sub>V</sub> is the valence-band edge, *E*<sub>F</sub> is the Fermi level with respect to *E*<sub>V</sub>, and  $\mu_N$  is the chemical potential of N [53], and *E*<sub>corr</sub> is the correction energy, which accounts for spurious interactions among charged defects within the periodic boundary condition.

In the present work, we consider only the monopole correction [54] using an average dielectric constant of 10, which is calculated by density-functional perturbation theory [55–57] applied on *a*-Si<sub>3</sub>N<sub>4</sub>. The correction energy is about 0.2 eV. For *E*<sup>0</sup>, we use the averaged total energy of stoichiometric *a*-Si<sub>3</sub>N<sub>4</sub>. Because of structural variations in the amorphous phase, direct comparison of the formation energy among different amorphous structures would be inappropriate. However, it does not change the distribution of *U* values since *U* is determined from the energy difference between two charge states and the contribution of *E*<sup>0</sup> cancels out.

We find that quite a few amorphous structures undergo unusually large relaxations when charged with one extra electron or one less electron, which should be caused by the metastability of amorphous structures. The repeated charge-discharge cycles on such defects always lead to distinct structures, obscuring the precise definition of the transition level. To exclude those defects for a clear interpretation, we perform stability tests in which the atomic structure is optimized during repeated (2–3 times) charging (*q* = +1 or −1) and discharging (*q* = 0) cycles, and choose samples whose structures (judged by eigenvalues in the Coulomb matrix [58]) remain almost identical with negligible changes in energy (less than 0.01 eV/cell) after charging-discharging cycles.

## III. RESULTS AND DISCUSSION

### A. Properties of stoichiometric *a*-Si<sub>3</sub>N<sub>4</sub>

We generate 40 *a*-Si<sub>3</sub>N<sub>4</sub> samples following the aforementioned melt-quench procedure. Figure 1(a) shows a typical structure of *a*-Si<sub>3</sub>N<sub>4</sub>, showing that fourfold (three-fold) coordination of Si (N) is well preserved as in *c*-Si<sub>3</sub>N<sub>4</sub>. (The average coordination numbers are 4.03 and 3.04 for Si and N atoms, respectively.) In Figs. 1(b) and 1(c), we plot average radial distribution functions (RDFs) for Si—N, Si—Si, and N—N, and angle distribution functions (ADFs) for Si—N—Si and N—Si—N. The first peak positions in Fig. 1(b) correspond to the average bond lengths, and they are compiled in Table I. The overall shape and main features of the calculated RDF and ADF agree well with previous DFT calculations [39,40] and experimental data [11,48]. For *a*-Si<sub>3</sub>N<sub>4</sub>, the Si—N RDF peaks at 1.75 Å, which is close to the first-neighbor distance in *c*-Si<sub>3</sub>N<sub>4</sub> (1.73 Å). The clear separation between the first peak and the second peak in the Si—N RDF indicates a rigid local structure that comes from the strong covalency of the Si—N bonds in *a*-Si<sub>3</sub>N<sub>4</sub>. The Si—Si RDF shows a main peak around 3.01 Å, which is attributed to the second-neighbor distance between Si atoms. Similarly, the first peak around 2.82 Å in the N—N RDF represents the distance between N atoms in second neighbors. In the Si—Si RDF, a small shoulder peak is noticeable around 2.5 Å, which has no corresponding bond in *c*-Si<sub>3</sub>N<sub>4</sub>. This peak

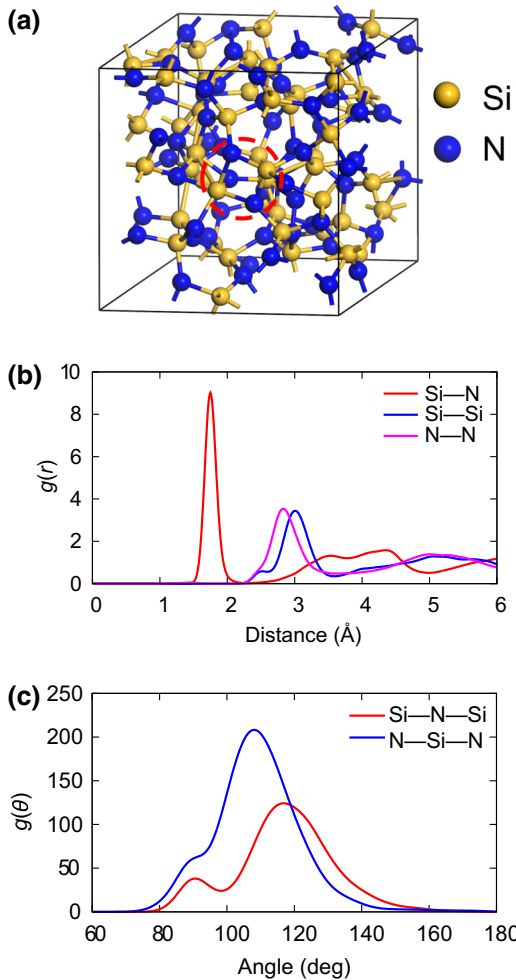


FIG. 1. (a) The atomic structure of the  $\alpha$ - $\text{Si}_3\text{N}_4$  unit cell. The dashed circle indicates a four-membered square ring. (b) Radial distribution functions. (c) Angle distribution functions.

originates from  $\text{Si}—\text{N}—\text{Si}—\text{N}$  square-ring structures, and one of them is indicated by a dashed circle in Fig. 1(a) [38,39]. There are six to 15 square rings for each sample. Although the square ring exists only in the amorphous structures, it does not produce any defect state within the band gap, because local coordinations of Si and N atoms are still the same as in  $c$ - $\text{Si}_3\text{N}_4$ .

In the  $\text{N}—\text{Si}—\text{N}$  ADF, the main peak is located around  $109^\circ$  as expected from the fourfold coordination and tetrahedral geometry of Si. In the  $\text{Si}—\text{N}—\text{Si}$  ADF, the main peak slightly shifts from  $120^\circ$  to a lower angle because the threefold-coordinated N atom can pucker slightly due to the lone pairs. This contrasts with N atoms in  $c$ - $\text{Si}_3\text{N}_4$ , which form planar units with neighboring Si atoms. The shoulder peaks at  $90^\circ$  are noticeable in both ADFs, which originates from the  $\text{Si}—\text{N}—\text{Si}—\text{N}$  square ring mentioned above.

Figure 2(a) shows the density of states (DOS) of  $\alpha$ - $\text{Si}_3\text{N}_4$  that is averaged over 40 samples generated independently.

TABLE I. Mean bonding distances in  $\alpha$ - $\text{Si}_3\text{N}_4$  compared with previous first-principles and experimental data (all values are in angstroms).

	$d(\text{Si}—\text{N})$	$d(\text{Si}—\text{Si})$	$d(\text{N}—\text{N})$
DFT [39]	1.75	2.99	2.89
DFT [59]	1.76	3.10	2.90
Experiment [11]	1.75	3.00	3.00
Experiment [48]	1.73	2.83	2.83
Present work	1.75	3.01	2.82

The DOS in each structure is aligned with respect to the averaged electrostatic potential at N sites [61]. The difference among samples is less than 0.1 eV. Since computing the DOS requires high-density sampling of  $\mathbf{k}$  points, direct application of the hybrid functional is formidable. Instead, the DOS in Fig. 2(a) is obtained from the PBE calculation with enough  $\mathbf{k}$ -point sampling, and the scissor correction is applied with use of complementary HSE06 calculations. To be specific, the correction is done by performing a  $\Gamma$ -only HSE06 calculation on each sample, and evaluating the average shift of eigenvalues at the band edge with respect to the PBE results. The resulting eigenvalue shifts are  $-0.95$  and  $0.40$  eV for occupied and unoccupied bands, respectively, giving a band-gap correction of  $1.35$  eV. The mobility edges ( $E_V$  and  $E_C$ ) and the corresponding band gap are obtained by fitting the DOS near band edges with square-root forms, as shown by the dashed lines in Fig. 2(a).

The band gap obtained from  $E_C - E_V$  is  $4.55$  eV, which is in good agreement with experimental data ( $4.0$ – $4.83$  eV) [60,62–65]. In comparison, the band gap of  $c$ - $\text{Si}_3\text{N}_4$  is  $5.47$  eV in the present HSE06 calculation. Another approach to estimate the band gap of amorphous structures is to calculate the optical absorption coefficient ( $\alpha$ ) as a function of photon energy ( $E_{\text{ph}}$ ) (the so-called Tauc plot), which is given as follows:

$$\alpha(E_{\text{ph}}) = \frac{\sqrt{2}E_{\text{ph}}}{\hbar} \left[ \sqrt{\epsilon_1^2(E_{\text{ph}}) + \epsilon_2^2(E_{\text{ph}})} - \epsilon_1(E_{\text{ph}}) \right]^{1/2}, \quad (2)$$

where  $\epsilon_1$  and  $\epsilon_2$  are real and imaginary parts of macroscopic dielectric functions, respectively [55,61]. In Fig. 2(b), it is seen that the theoretical Tauc plot compares favorably with the experimental result [60]. The extrapolated band gap is  $4.86$  eV, in reasonable agreement with  $4.55$  eV estimated directly from the DOS in Fig. 2(a).

## B. Atomic and electronic structures of $K$ centers in $\alpha$ - $\text{Si}_3\text{N}_{4-x}$

We generate 30  $\alpha$ - $\text{Si}_3\text{N}_{4-x}$  structures with the same melt-quench procedure as used to produce  $\alpha$ - $\text{Si}_3\text{N}_4$ . In

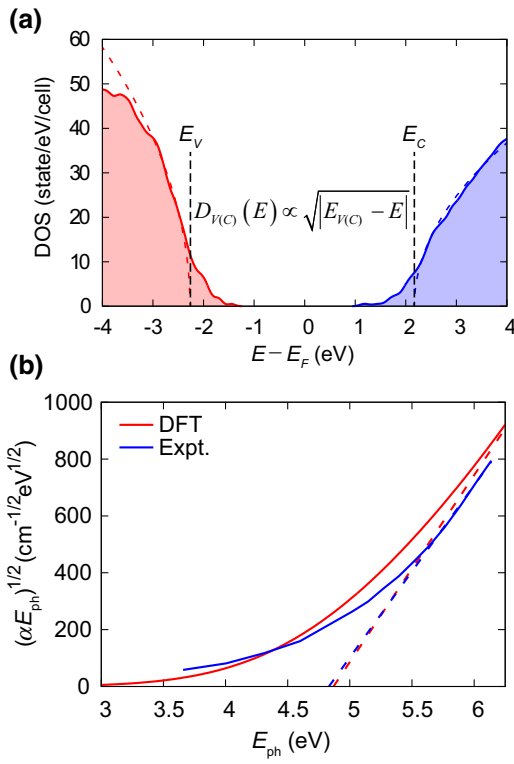


FIG. 2. (a) The DOS of  $a\text{-Si}_3\text{N}_4$  averaged over amorphous structures. The band edges are found by fitting the DOS near edges with square-root forms. (b) Tauc plot for  $a\text{-Si}_3\text{N}_4$ . The DFT band gap is corrected with the eigenvalue shift from the HSE06 calculation. The Tauc plot is also corrected with the HSE06-calculation result and compared with an experimental measurement [60].

$c\text{-Si}_3\text{N}_4$ , the nitrogen vacancy results in three undercoordinated Si atoms, which relax into one (stretched) Si—Si bond and one  $K$  center [30,31]. In the case of  $a\text{-Si}_3\text{N}_{4-x}$ , we find that most amorphous samples (21 of 30) contain one  $K$  center and one Si—Si bond after atomic relaxation, similar to  $c\text{-Si}_3\text{N}_4$ . In nine of 30 samples,  $a\text{-Si}_3\text{N}_{4-x}$  contains two Si—Si bonds or one Si—Si bond with an undercoordinated Si atom. However, they are usually unstable and transform into another structure during the charge-discharge test (see above). As such, we exclude them in the ensuing analysis. A representative atomic configuration of the  $K$  center is presented in Fig. 3(a) together with the Si—Si bond. Except for the defects, the structural properties of  $a\text{-Si}_3\text{N}_{4-x}$  are similar to those of  $a\text{-Si}_3\text{N}_4$ .

Figure 3(b) shows a typical electronic structure of  $a\text{-Si}_3\text{N}_{4-x}$  that contains the Si—Si bond and the  $K$  center as in Fig. 3(a). The partial DOS projected onto the Si—Si bond or the  $K$  center is also plotted. It is seen that the Si—Si bond does not form a distinct defect level within the band gap as the bonding and antibonding states localized at the Si—Si bond appear close to or inside the band. In contrast, the Si—Si bond in  $c\text{-Si}_3\text{N}_4$  produce the defect

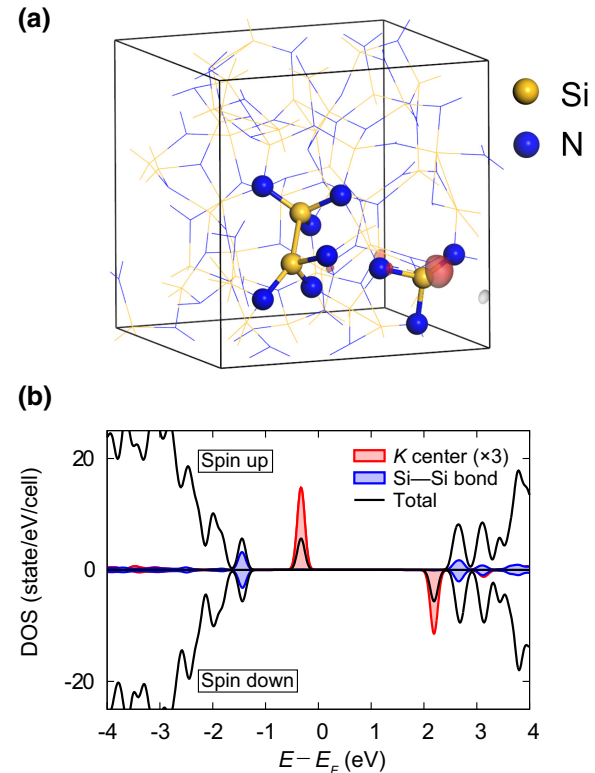


FIG. 3. (a) The atomic configuration of the representative  $a\text{-Si}_3\text{N}_{4-x}$ . For visual clarity, atoms except for those in the Si—Si bond and  $K$  center are drawn in wire frames. The semitransparent isosurface represents the defect level of the  $K$  center. (b) The spin-resolved total DOS and partial DOS projected on the  $K$  center and the Si—Si bond.

level located 1.2–1.4 eV from the conduction band minimum (CBM) [29–31]. This difference can be explained by the Si—Si bond length; the bond lengths of Si—Si in  $a\text{-Si}_3\text{N}_{4-x}$  are 2.3–2.5 Å, close to the bond length in crystalline Si (2.35 Å), while the Si—Si bond in  $c\text{-Si}_3\text{N}_4$  is significantly stretched (2.64 Å) because the crystalline backbone limits the relaxation of the two Si atoms. As such, the bonding-antibonding splitting in Si—Si is much larger in amorphous structures than in crystalline structures.

The Si—Si bond in  $a\text{-SiO}_2$  is known to be flexible and able to trap electrons [66]. To examine this possibility in the present system, we stretch the Si—Si bond until its antibonding state is pulled down below the empty level of the  $K$  center (other atoms are relaxed). We then occupy this state with one extra electron and perform full atomic relaxations. The stretched Si—Si bond shrinks back to the initial length and the antibonding state rises such that the extra electron is trapped again at the  $K$  center.

It is also noteworthy that in the amorphous phase the Si—Si bond and the  $K$  center are spatially well separated (the mean distance is approximately 5 Å), while in  $c\text{-Si}_3\text{N}_4$ , the two defect structures are close to each other and slightly

hybridized. This implies that the electronic property of the  $K$  center in the amorphous phase can be different from that in the crystalline phase, despite similarity in the local structure.

### C. Transition-level diagram

To obtain the transition level of  $K$  centers in  $a\text{-Si}_3\text{N}_{4-x}$ , we add or subtract one electron for 14 samples that include one  $K$  center and are stable under repeated cycles of charge and discharge (see Sec. II C). When positively charged, the pyramidal structure of the  $K$  center relaxes into a more-planar configuration. Accordingly, the average bond angle ( $\text{N}—\text{Si}—\text{N}$ ) increases from  $109.4^\circ$  to  $116.2^\circ$ . In contrast, the negative charging results in a sharper pyramid with the average bond angle decreasing to  $104.7^\circ$ . A similar relaxation pattern was observed for the  $K$  center in  $c\text{-Si}_3\text{N}_4$  [31].

The transition level of the charged defect is defined as the Fermi level at which the formation energies of different charge states coincide. From the definition of the formation energy in Eq. (1), the transition level from charge state  $q$  to charge state  $q'$  [ $\epsilon_t(q/q')$ ] can be estimated as follows:

$$\epsilon_t(q/q') = \frac{E^q - E^{q'}}{q' - q} - E_V. \quad (3)$$

The calculated transition levels for each sample are displayed in Fig. 4. The filled circles and squares indicate  $\epsilon_t(+1/0)$  and  $\epsilon_t(0/-1)$ , and the red, white, and blue bands mean Fermi level ranges at which  $K^+$ ,  $K^0$ , and  $K^-$  are most stable.  $U$  is equal to  $\epsilon_t(0/-1) - \epsilon_t(+1/0)$ , and the interval shown as the white area in each bar corresponds to positive  $U$ , while negative  $U$  is expressed as the overlap of the red and blue regions. As in averaging the DOS,  $E_F$  values among different amorphous structures are aligned with respect to the average potential values at the N site. The samples are arranged in decreasing order of  $U$  (see the top of Fig. 4).

In Fig. 4, it is seen that  $U$  varies over a wide range from  $-1.14$  to  $1.11$  eV. Most samples (ten of 14) show positive  $U$  values, while only four samples have negative ones. (The average value is  $0.37$  eV.) As mentioned above,  $U$  for the  $K$  center in the crystalline phase is very small (approximately  $-0.1$  eV), and therefore small variations in the local structure as in  $a\text{-Si}_3\text{N}_4$  can easily shift  $U$  to a positive value. In particular, the  $K$  center and Si—Si bond are apart from each other in  $a\text{-Si}_3\text{N}_{4-x}$ , and hence the neutral  $K$  center is spatially more relaxed than in  $c\text{-Si}_3\text{N}_4$ . These structural differences are expected to stabilize the  $K$  center, lowering the energy of  $K^0$  and resulting in positive- $U$  behavior.

In Fig. 4, it is also intriguing that the transition level varies from sample to sample, which is a consequence of variations in the local structure of  $K$  centers in the amorphous phase. In actual  $a\text{-Si}_3\text{N}_{4-x}$ ,  $K$  centers with different

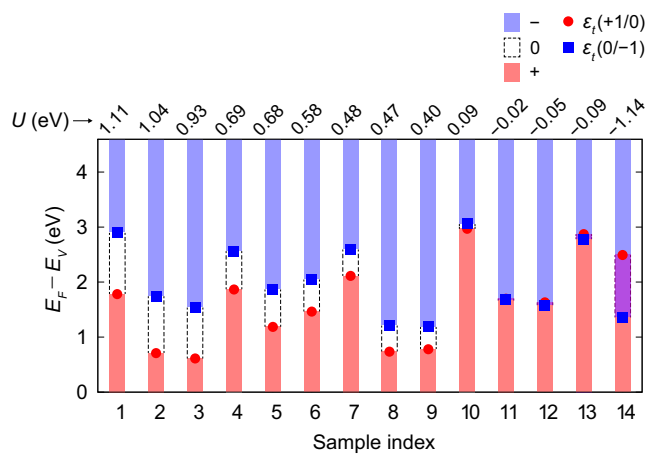


FIG. 4. Charge transition levels of the  $K$  center in each sample. The  $U$  values of the samples are shown at the top of each bar. The red circles and blue squares represent the transition level  $\epsilon_t(+1/0)$  and  $\epsilon_t(0/-1)$ , respectively [see Eq. (3)]. In each bar, the red and blue regions indicate the Fermi-level range at which the  $K$  center is charged positive and negative, respectively.

transition levels would coexist. This also means that the Fermi level will be determined by the charge equilibration among  $K$  centers. To illustrate this more clearly, we plot in Fig. 5(a) formation energies for two hypothetical  $K$  centers ( $K1$  and  $K2$ ). We suppose that  $K1$  and  $K2$  are the only defects in the system and both  $K$  centers have positive  $U$  values but their transition levels are different, with  $\epsilon_t^1$  and  $\epsilon_t^2$  being the transition levels for  $K1$  and  $K2$ , respectively. When the Fermi level is below  $\epsilon_t^1(+1/0)$ , both  $K$  centers are charged as  $+1$ , rendering the total charge of the system  $+2$ . As the Fermi level increases and passes  $\epsilon_t^1(+1/0)$ ,  $K1$  becomes neutral and the total charge of the system changes to  $+1$ . When the Fermi level lies between  $\epsilon_t^1(0/-1)$  and  $\epsilon_t^2(+1/0)$ ,  $K1$  is negatively charged, while  $K2$  is still positive, and the total charge of the system becomes zero. By the same token, the total charge of the system decreases to  $-1$  and  $-2$  as the Fermi level increases above  $\epsilon_t^2(+1/0)$  and  $\epsilon_t^2(0/-1)$ .

The interval between  $\epsilon_t^1(0/-1)$  and  $\epsilon_t^2(+1/0)$  [see the shaded region in Figs. 5(a) and 5(b)] corresponds to the charge-neutrality level in which the net charge of the whole system is zero. (We recall that the main focus of the present study is the charge states in the as-deposited neutral samples on which ESR measurements are performed. In such samples, the Fermi level is determined thermodynamically by imposing the charge-neutrality condition.) Even though both defects have positive  $U$ ,  $K1$  and  $K2$  are negatively and positively charged, respectively, at the charge-neutrality condition. The spontaneous charging of  $K$  centers may appear to show negative- $U$  behavior, and this is a result of different transition levels among the defects in disordered phases.

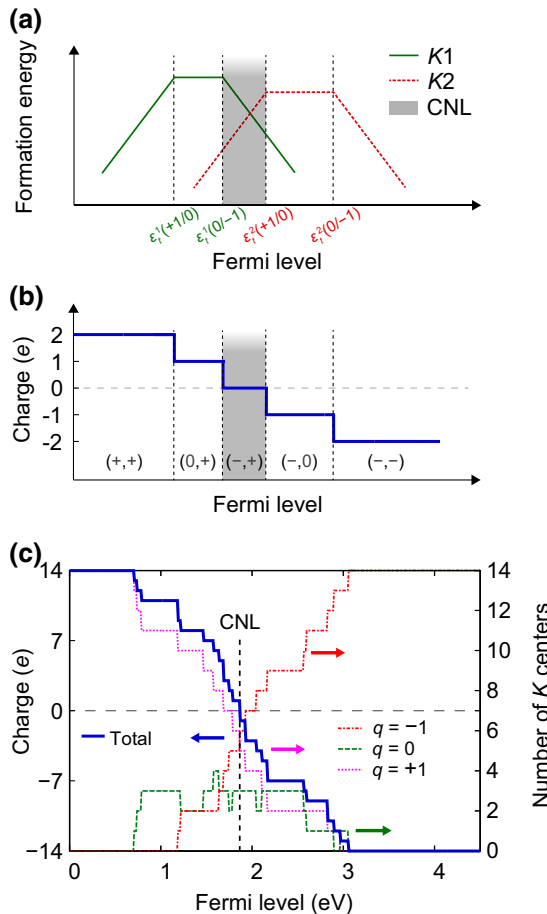


FIG. 5. (a) Formation-energy diagram of two hypothetical  $K$  centers ( $K1$  and  $K2$ ) that are assumed to be the only defects in the system. The solid green line and the dotted red line indicate the formation energy of  $K1$  and  $K2$  as a function of the Fermi level, respectively. The shaded region represents the Fermi-level range satisfying the neutrality condition of the total charge. (b) The total charge of the same system as a function of the Fermi level. The charge state of  $K1$  and  $K2$  in each region is given in parentheses. (c) The total charge for the ensemble of  $K$  centers in Fig. 4 as a function of  $E_F - E_V$ . The solid line is the total charge (left axis) and the other lines indicate the number of  $K$  centers in a certain charge state (right axis). CNL, charge-neutrality level.

For the collection of  $K$  centers in Fig. 4, one can count the number of  $K$  centers in each charge state as a function of the Fermi level, as shown in Fig. 5(c). The number of  $K$  centers in the  $q = -1$  state increases as the Fermi level increases, while that in the  $q = +1$  state decreases. The charge-neutrality level can be obtained as the Fermi level where the total charge of the system is zero, which is found to be approximately 1.9 eV above  $E_V$  [see the dashed line in Fig. 5(c)]. As a consequence, most of the traps (11 of 14) are in charged states even though most  $K$  centers show positive  $U$  individually. This seemingly negative- $U$  behavior is consistent with experimental reports in which the trap states act as diamagnetic centers ( $K^+$  or  $K^-$ ) under

ESR measurement, without the intrinsic negative- $U$  nature being invoked.

In passing, we note that the charge transition level can be sensitive to the supercell size because of possible long-range relaxations [67]. Since the size test with amorphous structures is too expensive due to the melt-quench process, we alternatively compare the charge transition levels of the N vacancy in  $c\text{-Si}_3\text{N}_4$  with different numbers of atoms (from 83 to 503 atoms). The transition levels calculated with 111 atoms converge to the results with 503 atoms within approximately 0.1 eV. Albeit indirect, this may support the use of amorphous models with 111 atoms.

#### D. Charge-trap levels

With the conditions identified in the previous subsection, we estimate the charge-trap level within the band gap. The energy level of electron trapping is defined as the Fermi level over which the charge state of the given defect changes. The charge injection from the electrode to the defect occurs mainly through a tunneling mechanism [68]. By investigating multiphonon-assisted tunneling, we find that the injection rate is maximum with a phonon emission of  $S\hbar\omega$ , where  $S$  is the Huang-Rhys factor and  $\hbar\omega$  is the phonon energy in the single-mode approximation. We refer to the formalism developed in Refs. [69,70] and use the Huang-Rhys factors and phonon energy found for point defects in semiconductors [71,72] (see Supplemental Material [73] for details). Classically, this corresponds to the Franck-Condon approximation in which the charge trapping occurs instantaneously while the atomic positions are fixed to those at equilibrium before injection [74]. Thus, the trap level can be estimated by following the method for the thermodynamic transition level, except that the charge trapping does not accompany atomic relaxations. (A similar approach was adopted to estimate the charge-trap level in  $\text{HfO}_2$ , agreeing well with the experimental results [75]. We also note that such Franck-Condon behavior was confirmed in the charge trapping in  $\text{SiO}_2$  [76].) Taking this into account, we can express the charging level from  $q$  to  $q \pm 1$  [ $\epsilon_i(q/q \pm 1)$ ] as

$$\epsilon_i(q/q \pm 1) = \pm(E^q - E_q^{q \pm 1}) - E_V, \quad (4)$$

where  $E_q^{q \pm 1}$  denotes the energy of the atomic structure relaxed at  $q$  but charged as  $q \pm 1$ . In Eq. (4),  $q + 1$  ( $q - 1$ ) indicates hole (electron) injection. The charge-trap levels for electrons and holes calculated from Eq. (4) are shown in Fig. 6. Here we consider not only the  $q = 0$  to  $-1$  ( $q = 0$  to  $+1$ ) transition but also the  $q = +1$  to  $0$  ( $q = -1$  to  $0$ ) transition for electron (hole) trapping, because in the charge-neutrality condition the relevant state of the  $K$  center in which the electron (hole) is trapped is mostly  $K^+$  ( $K^-$ ). The distribution of the trap level spreads over approximately 1.0 eV because of variations in the local

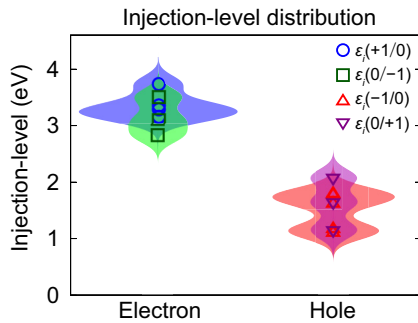


FIG. 6. Distribution of charge-trap levels in  $a\text{-Si}_3\text{N}_{4-x}$  plotted with Gaussian smearing with  $\sigma = 0.15$  eV.

structure of the  $K$  center. The electron-trap level peaks at 1.35 eV from the CBM and averages around 1.33 eV. On the other hand, the hole-trap level is 1.54 eV from the valence band maximum on average.

The experimental measurement of the trap distribution has been performed with various methods, including thermally stimulated exoelectron emission [77], current-voltage-characteristic analysis [78], and trap spectroscopy with charge injection and sensing (TSCIS) [79]. Among these, TSCIS measurement is closely related to the situation in CTF memory since it measures the injection voltage at which the tunneling of carriers occurs. In TSCIS, the threshold voltage shift from charge injection is measured while the injection voltage and injection time are swept, which enables the spatial detection of the defect band profile from the conduction-band edge [79]. The trap levels reported for Si-rich  $a\text{-Si}_3\text{N}_4$  are 1.1–1.5 eV below the CBM and peak at approximately 1.4 eV [80], which agrees well with our theoretical estimation of 1.35 eV. Since the hole-injection level from TSCIS is not available, we compare our result of 1.54 eV against the hole-trap level of approximately 1.4 eV estimated from voltage-current characteristics, which also shows good agreement [78].

#### IV. CONCLUSION

In summary, the nature of  $K$  centers in  $a\text{-Si}_3\text{N}_{4-x}$  is studied with first-principles calculations based on DFT and a hybrid functional. The negative- $U$  character of the  $K$  center, which is supported by ESR experiments and theoretical studies on the crystalline phase, is revisited. Among the Si–Si bond and the  $K$  center generated by melt-quench processes, only the  $K$  center is able to act as a trap center in the amorphous phase. The calculated  $U$  for the  $K$  center ranges widely from –1.14 to 1.11 eV. Although individual  $K$  centers display mostly positive  $U$ , the charge-neutrality condition imposed on the ensemble of  $K$  centers results in seemingly negative- $U$  behavior. Therefore, the negative- $U$  behavior of  $a\text{-Si}_3\text{N}_{4-x}$  can be understood as originating from the disorder in the local structure of  $K$  centers in the amorphous phase rather than the intrinsic negative- $U$

property of each  $K$  center. We calculated charge-trap levels for electrons and holes, and the theoretical estimation is in close agreement with extant experimental data. We believe that the present work provides an alternative aspect in the charge-trapping behavior of amorphous materials, serving as a key to improve the performance of charge-trap devices.

#### ACKNOWLEDGMENTS

This work was supported by a research project of SK Hynix Inc. and the Industrial Strategic Technology Development Program (No. 10052925, Atomistic process and device modeling of sub-10 nm scale transistors) funded by the Ministry of Trade, Industry & Energy (Korea). The computations were performed at the KISTI supercomputing center (Grant No. KSC-2018-C3-0022).

- [1] J. S. Meena, S. M. Sze, U. Chand, and T.-Y. Tseng, Overview of emerging nonvolatile memory technologies, *Nanoscale Res. Lett.* **9**, 526 (2014).
- [2] K. Sonoda, E. Tsukuda, M. Tanizawa, and Y. Yamaguchi, Electron trap level of hydrogen incorporated nitrogen vacancies in silicon nitride, *J. Appl. Phys.* **117**, 104501 (2015).
- [3] W. Jang, H. Jeon, C. Kang, H. Song, J. Park, H. Kim, H. Seo, M. Leskela, and H. Jeon, Temperature dependence of silicon nitride deposited by remote plasma atomic layer deposition, *Phys. Status Solidi A* **211**, 2166 (2014).
- [4] D.-H. Lee, K.-T. Lim, E.-K. Park, H.-C. Shin, C. S. Kim, K.-C. Park, J.-R. Ahn, J. H. Bang, and Y.-S. Kim, Investigation of charge trapping mechanism for nanocrystal-based organic nonvolatile floating gate memory devices by band structure analysis, *Electron. Mater. Lett.* **12**, 376 (2016).
- [5] L. Wang, C.-H. Yang, and J. Wen, Physical principles and current status of emerging non-volatile solid state memories, *Electron. Mater. Lett.* **11**, 505 (2015).
- [6] F. Yoshihisa, Review of emerging new solid-state non-volatile memories, *Jpn. J. Appl. Phys.* **52**, 040001 (2013).
- [7] T. L. Chu, J. R. Szedon, and C. H. Lee, The preparation and C-V characteristics of Si– $\text{Si}_3\text{N}_4$  and Si– $\text{SiO}_2$ – $\text{Si}_3\text{N}_4$  structures, *Solid-State Electron.* **10**, 897 (1967).
- [8] S. M. Hu, D. R. Kerr, and L. V. Gregor, Evidence of hole injection and trapping in silicon nitride films prepared by reactive sputtering, *Appl. Phys. Lett.* **10**, 97 (1967).
- [9] H. C. Pao and M. O'Connell, Memory behavior of an MNS capacitor, *Appl. Phys. Lett.* **12**, 260 (1968).
- [10] F. A. Sewell, Jr., H. A. R. Wegener, and E. T. Lewis, Charge storage model for variable threshold FET memory element, *Appl. Phys. Lett.* **14**, 45 (1969).
- [11] T. Aiyama, T. Fukunaga, K. Niihara, T. Hirai, and K. Suzuki, An X-ray diffraction study of the amorphous structure of chemically vapor-deposited silicon nitride, *J. Non-Cryst. Solids* **33**, 131 (1979).
- [12] J. Robertson and M. J. Powell, Gap states in silicon nitride, *Appl. Phys. Lett.* **44**, 415 (1984).

- [13] C. T. Kirk, Jr., Valence alternation pair model of charge storage in MNOS memory devices, *J. Appl. Phys.* **50**, 4190 (1979).
- [14] K. L. Ngai and Y. Hsia, Empirical study of the metal-nitride-oxide-semiconductor device characteristics deduced from a microscopic model of memory traps, *Appl. Phys. Lett.* **41**, 159 (1982).
- [15] N. H. Nickel, W. B. Jackson, and N. M. Johnson, Light-Induced Creation of Metastable Paramagnetic Defects in Hydrogenated Polycrystalline Silicon, *Phys. Rev. Lett.* **71**, 2733 (1993).
- [16] W. M. Pontuschka, W. W. Carlos, P. C. Taylor, and R. W. Griffith, Radiation-induced paramagnetism in *a*-Si:H, *Phys. Rev. B* **25**, 4362 (1982).
- [17] D. K. Biegelsen and M. Stutzmann, Hyperfine studies of dangling bonds in amorphous silicon, *Phys. Rev. B* **33**, 3006 (1986).
- [18] S. Fujita and A. Sasaki, Dangling bonds in memory-quality silicon nitride films, *J. Electrochem. Soc.* **132**, 398 (1985).
- [19] D. T. Krick, P. M. Lenahan, and J. Kanicki, Electrically active point defects in amorphous silicon nitride: An illumination and charge injection study, *J. Appl. Phys.* **64**, 3558 (1988).
- [20] D. Jousse, D. Kanicki, and J. H. Stathis, Observation of multiple silicon dangling bond configurations in silicon nitride, *Appl. Phys. Lett.* **54**, 1043 (1989).
- [21] P. M. Lenahan, D. T. Krick, and J. Kanicki, The nature of the dominant deep trap in amorphous silicon nitride films: Evidence for a negative correlation energy, *J. Appl. Surf. Sci.* **39**, 392 (1989).
- [22] W. L. Warren, J. Kanicki, F. C. Rong, and E. H. Poindexter, Paramagnetic point defects in amorphous silicon dioxide and amorphous silicon nitride thin films, *J. Electrochem. Soc.* **139**, 880 (1992).
- [23] S. Hasegawa, M. Matsuda, and Y. Kurata, Bonding configuration and defects in amorphous SiN<sub>x</sub>:H films, *Appl. Phys. Lett.* **58**, 741 (1991).
- [24] W. L. Warren, J. Kanicki, J. Robertson, E. H. Poindexter, and P. J. McWhorter, Electron paramagnetic resonance investigation of charge trapping centers in amorphous silicon nitride films, *J. Appl. Phys.* **74**, 4034 (1993).
- [25] G. Pacchioni and D. Erbetta, Electronic structure and spectral properties of paramagnetic point defects in Si<sub>3</sub>N<sub>4</sub>, *Phys. Rev. B* **60**, 12617 (1999).
- [26] V. A. Gritsenko, Yu. N. Novikov, A. V. Shaposhnikov, and Yu. N. Morokov, Numerical simulation of intrinsic defects in SiO<sub>2</sub> and Si<sub>3</sub>N<sub>4</sub>, *Semiconductors* **35**, 997 (2001).
- [27] M. Petersen and Y. Roizin, Density functional theory study of deep traps in silicon nitride memories, *Appl. Phys. Lett.* **89**, 053511 (2006).
- [28] V. A. Gritsenko, S. S. Nekrashevich, V. V. Vasilev, and A. V. Shaposhnikov, Electronic structure of memory traps in silicon nitride, *Microelectron. Eng.* **86**, 1866 (2009).
- [29] M. E. Grillo, S. D. Elliott, and C. Freysoldt, Native defects in hexagonal  $\beta$ -Si<sub>3</sub>N<sub>4</sub> studied using density functional theory calculations, *Phys. Rev. B* **83**, 085208 (2011).
- [30] E. Vianello, F. Driussi, L. Perniola, G. Molas, J. Colonna, B. De Salvo, and L. Selmi, Explanation of the charge trapping properties of silicon nitride storage layers for NVMs-part II: Atomistic and electrical modeling, *IEEE Trans. Electron Devices* **58**, 2490 (2011).
- [31] C. D. Valentini, G. Palma, and G. Pacchioni, Ab initio study of transition levels for intrinsic defects in silicon nitride, *J. Phys. Chem. C* **115**, 561 (2011).
- [32] W. S. Patrocínio, M. Ribeiro, Jr., and L. R. C. Fonseca, Theoretical study of charge trapping levels in silicon nitride using the LDA-1/2 self-energy correction scheme for excited states, *Mater. Sci. Eng. B* **177**, 1497 (2012).
- [33] V. A. Gritsenko, Yu. N. Novikov, A. V. Shaposhnikov, H. Wong, and G. M. Zhidomirov, Capturing properties of a threefold coordinated silicon atom in silicon nitride: Positive correlation energy model, *Phys. Solid State* **45**, 2031 (2003).
- [34] P. Kroll, Structure and reactivity of amorphous silicon nitride investigated with density-functional methods, *J. Non-Cryst. Solids* **293–295**, 238 (2001).
- [35] F. Alvarez and A. A. Valladares, Optical gaps of ab initio generated random networks for *a*-SiN<sub>x</sub> alloys, *Appl. Phys. Lett.* **80**, 58 (2002).
- [36] F. Alvarez, C. C. Díaz, A. A. Valladares, and R. M. Valladares, Radial distribution functions of ab initio generated amorphous covalent networks, *Phys. Rev. B* **65**, 113108 (2002).
- [37] J. F. Justo, F. de Brito Mota, and A. Fazzio, First-principles investigation of *a*-SiN<sub>x</sub>:H, *Phys. Rev. B* **65**, 073202 (2002).
- [38] L. Giacomazzi and P. Umari, First-principles investigation of electronic, structural, and vibrational properties of *a*-Si<sub>3</sub>N<sub>4</sub>, *Phys. Rev. B* **80**, 144201 (2009).
- [39] L. E. Hintzsche, C. M. Fang, T. Watts, M. Marsman, G. Jordan, M. W. P. E. Lamers, A. W. Weeber, and G. Kresse, Density functional theory study of the structural and electronic properties of amorphous silicon nitrides: Si<sub>3</sub>N<sub>4-x</sub>:H, *Phys. Rev. B* **86**, 235204 (2012).
- [40] L. E. Hintzsche, C. M. Fang, M. Marsman, G. Jordan, M. W. P. E. Lamers, A. W. Weeber, and G. Kresse, Defects and defect healing in amorphous Si<sub>3</sub>N<sub>4-x</sub>H<sub>y</sub>: An ab initio density functional theory study, *Phys. Rev. B* **88**, 155204 (2013).
- [41] R. P. Vedula, S. Palit, M. A. Alam, and A. Strachan, Role of atomic variability in dielectric charging: A first-principles-based multiscale modeling study, *Phys. Rev. B* **88**, 205204 (2013).
- [42] G. Kresse and J. Furthmüller, Efficient iterative schemes for ab initio total-energy calculations using a plane-wave basis set, *Phys. Rev. B* **54**, 11169 (1996).
- [43] G. Kresse and J. Furthmüller, Efficiency of ab-initio total energy calculations for metals and semiconductors using a plane-wave basis set, *Comput. Mater. Sci.* **6**, 15 (1996).
- [44] P. E. Blöchl, Projector augmented-wave method, *Phys. Rev. B* **50**, 17953 (1994).
- [45] J. P. Perdew, K. Burke, and M. Ernzerhof, Generalized gradient approximation made simple, *Phys. Rev. Lett.* **77**, 3865 (1996).
- [46] J. Heyd, G. E. Scuseria, and M. Ernzerhof, Hybrid functionals based on a screened Coulomb potential, *J. Chem. Phys.* **118**, 8207 (2003).
- [47] Y. Youn, Y. Kang, and S. Han, An efficient method to generate amorphous structures based on local geometry, *Comput. Mater. Sci.* **95**, 256 (2014).

- [48] M. Misawa, T. Fukunaga, K. Niihara, T. Hirai, and K. Suzuki, Structural study of amorphous  $\text{SiN}_x$  : H films produced by plasma-enhanced chemical vapor deposition, *J. Non-Cryst. Solids* **34**, 313 (1979).
- [49] M. M. Guraya, H. Ascolani, G. Zampieri, J. I. Cisneros, J. H. Dias da Silva, and M. P. Cantão, Bond densities and electronic structure of amorphous  $\text{SiN}_x$  : H, *Phys. Rev. B* **42**, 5677 (1990).
- [50] R. E. I. Schropp, S. Nishizaki, Z. Houweling, V. Verlaan, C. H. M. van der Werf, and H. Matsumura, All hot wire CVD TFTs with high deposition rate silicon nitride (3 nm/s), *Solid-State Electron.* **52**, 427 (2008).
- [51] F. Giorgis, C. F. Pirri, and E. Tresso, Structural properties of  $a\text{-Si}_{1-x}\text{N}_x\text{:H}$  films grown by plasma enhanced chemical vapour deposition by  $\text{SiH}_4 + \text{NH}_3 + \text{H}_2$  gas mixtures, *Thin Solid Films* **307**, 298 (1997).
- [52] R. P. Vedula, N. L. Anderson, and A. Strachan, Effect of topological disorder on structural, mechanical, and electronic properties of amorphous silicon nitride: An atomistic study, *Phys. Rev. B* **85**, 205209 (2012).
- [53] C. Freysoldt, B. Grabowski, T. Hückel, J. Neugebauer, G. Kresse, A. Janotti, and C. G. Van de Walle, First-principles calculations for point defects in solids, *Rev. Mod. Phys.* **86**, 253 (2014).
- [54] G. Makov and M. C. Payne, Periodic boundary conditions in ab initio calculations, *Phys. Rev. B* **51**, 4014 (1995).
- [55] M. Gajdoš, K. Hummer, G. Kresse, J. Furthmüller, and F. Bechstedt, Linear optical properties in the projector-augmented wave methodology, *Phys. Rev. B* **73**, 045112 (2006).
- [56] S. Baroni and R. Resta, Ab initio calculation of the macroscopic dielectric constant in silicon, *Phys. Rev. B* **33**, 7017 (1986).
- [57] X. Wu, D. Vanderbilt, and D. R. Hamann, Systematic treatment of displacements, strains, and electric fields in density-functional perturbation theory, *Phys. Rev. B* **72**, 035105 (2005).
- [58] K. T. Schütt, H. Glawe, F. Brockherde, A. Sanna, K. R. Müller, and E. K. U. Gross, How to represent crystal structures for machine learning: Towards fast prediction of electronic properties, *Phys. Rev. B* **89**, 205118 (2014).
- [59] K. Jarolimek, R. A. deGroot, G. A. de Wijs, and M. Zeman, Atomistic models of hydrogenated amorphous silicon nitride from first principles, *Phys. Rev. B* **82**, 205201 (2010).
- [60] J. Cisneros, Optical characterization of dielectric and semiconductor thin films by use of transmission data, *Appl. Opt.* **37**, 5262 (1998).
- [61] Y. Kang, H. Song, H.-H. Nahm, S. H. Jeon, Y. Cho, and S. Han, Intrinsic nature of visible-light absorption in amorphous semiconducting oxides, *APL Mater.* **2**, 032108 (2014).
- [62] S. Yerci, R. Li, S. O. Kucheyev, T. van Buuren, S. N. Basu, and L. D. Negro, Visible and  $1.54\text{ }\mu\text{m}$  emission from amorphous silicon nitride films by reactive cosputtering, *IEEE J. Sel. Top. Quantum Electron.* **16**, 114 (2010).
- [63] A. V. Vishnyakov, Yu. N. Novikov, V. A. Gritsenko, and K. A. Nasirov, The charge transport mechanism in silicon nitride: Multi-phonon trap ionization, *Solid-State Electron.* **53**, 251 (2009).
- [64] R. Kärcher, L. Ley, and R. L. Johnson, Electronic structure of hydrogenated and unhydrogenated amorphous  $\text{SiN}_x$  ( $0 \leq x \leq 1.6$ ): A photoemission study, *Phys. Rev. B* **30**, 1896 (1984).
- [65] J. F. Lelièvre, J. De la Torre, A. Kaminski, G. Bremond, M. Lemiti, R. El Bouayadi, D. Araujo, T. Epicier, R. Monna, M. Pirot, P. J. Ribeyron, and C. Jaussaud, Correlation of optical and photoluminescence properties in amorphous  $\text{SiN}_x$  : H thin films deposited by PECVD or UVCVD, *Thin Solid Films* **511**, 103 (2006).
- [66] J. P. Vigouroux, J. P. Duraud, A. Le Moel, C. Le Gressus, and D. L. Griscom, Electron trapping in amorphous  $\text{SiO}_2$  studied by charge buildup under electron bombardment, *J. Appl. Phys.* **57**, 5139 (1985).
- [67] V. B. Sulimov, P. V. Sushko, A. H. Edwards, A. L. Shluger, and A. M. Stoneham, Asymmetry and long-range character of lattice deformation by neutral oxygen vacancy in  $\alpha$ -quartz, *Phys. Rev. B* **66**, 024108 (2002).
- [68] H. Fecht and M. Werner, *The nano-micro interface: Bridging the micro and nano worlds* (Wiley-VCH, Weinheim, 2004).
- [69] M. Herrmann and A. Schenk, Field and high-temperature dependence of the long term charge loss in erasable programmable read only memories: Measurements and modeling, *J. Appl. Phys.* **77**, 4522 (1995).
- [70] G. Jegert, A. Kersch, W. Weinreich, U. Schröder, and P. Lugli, Modeling of leakage currents in high- $\kappa$  dielectrics: Three-dimensional approach via kinetic Monte Carlo, *Appl. Phys. Lett.* **96**, 062113 (2010).
- [71] A. Alkauskas, J. L. Lyons, D. Steiauf, and C. G. Van de Walle, First-Principles Calculations of Luminescence Spectrum Line Shapes for Defects in Semiconductors: The Example of GaN and ZnO, *Phys. Rev. Lett.* **109**, 267401 (2012).
- [72] A. Alkauskas, Q. Yan, and C. G. Van de Walle, First-principles theory of nonradiative carrier capture via multiphonon emission, *Phys. Rev. B* **90**, 075202 (2014).
- [73] See Supplemental Material at <http://link.aps.org/supplemental/10.1103/PhysRevApplied.10.064052> for details of the modeling of multiphonon-assisted tunneling and discussion of the Franck-Condon approximation.
- [74] W. Goes, Y. Wimmer, A.-M. El-Sayed, G. Rzepa, M. Jech, A. L. Shluger, and T. Grasser, Identification of oxide defects in semiconductor devices: A systematic approach linking DFT to rate equations and experimental evidence, *Microel. Reliab.* **87**, 286 (2018).
- [75] P. Broqvist and A. Pasquarello, Oxygen vacancy in monoclinic  $\text{HfO}_2$ : A consistent interpretation of trap assisted conduction, direct electron injection, and optical absorption experiments, *Appl. Phys. Lett.* **89**, 262904 (2006).
- [76] W. B. Fowler, J. K. Rudra, M. E. Zvanut, and F. J. Feigl, Hysteresis and Franck-Condon relaxation in insulator-semiconductor tunneling, *Phys. Rev. B* **41**, 8313 (1990).
- [77] S. Heo, H. Park, J. Chung, H. I. Lee, J. Park, Y. K. Kyoung, Y. S. Kim, K. Kim, S. Byun, W. S. Jeon, G. S. Park, P. Choi, B.-D. Choi, D. Lee, H. Y. Cho, and H. J. Kang, Defect states in amorphous  $\text{SiN}_x\text{:H}$  compounds using thermally stimulated exo-electron emission, *Thin Solid Films* **616**, 850 (2016).

- [78] V. A. Gritsenko, T. V. Perevalov, O. M. Orlov, and G. Ya. Krasnikov, Nature of traps responsible for the memory effect in silicon nitride, *Appl. Phys. Lett.* **109**, 062904 (2016).
- [79] M. Cho, R. Degraeve, P. Roussel, B. Govoreanu, B. Kaczer, M. B. Zahid, E. Simoen, A. Arreghini, M. Jurczak, J. Van Houdt, and G. Groeseneken, A consistent model for oxide trap profiling with the trap spectroscopy by charge injection and sensing (TSCIS) technique, *Solid-State Electron.* **54**, 1384 (2010).
- [80] A. Suhane, A. Arreghini, R. Degraeve, G. Van den bosch, L. Breuil, M. B. Zahid, M. Jurczak, K. De Meyer, and J. VanHoudt, Validation of retention modeling as a trap-profiling technique for SiN-based charge-trapping memories, *IEEE Electron Device Lett.* **31**, 77 (2010).